OPTIMIZED INTERPRETATION OF SAGEEP 2011 BLIND REFRACTION DATA WITH FRESNEL VOLUME TOMOGRAPHY AND PLUS-MINUS REFRACTION

Siegfried R.C. Rohdewald, Intelligent Resources Inc., Vancouver BC, Canada

Abstract

We improve the resolution of subsurface P-wave velocity tomograms with Fresnel Volume Tomography and Wavepath Eikonal Traveltime inversion, by iteratively decreasing the wavepath width. We use the SAGEEP 2011 blind refraction synthetic traveltime data to compare our tomograms with the known true model. We compare weighting of the wavepath velocity update with a Ricker wavelet vs. weighting with a Gaussian bell function. Plotting Plus-Minus refractors obtained with layer-based interpretation on the 2D velocity tomogram better visualizes both methods. Tomograms from an iterative approach of wavepath adjustment show improvement over the standard ray-based method.

Introduction

Wavepath Eikonal Traveltime inversion

Wavepath Eikonal Traveltime (WET) inversion (Schuster and Quintus-Bosz, 1993; Sheehan et al., 2005; Rohdewald et al., 2010; Rohdewald, 2011) uses the Fresnel volume approach (Watanabe et al., 1999) to model propagation of first-break energy in a physically realistic way. Ray-tracing methods assume that the frequency of the source signal is infinite and model wave propagation along “thin rays”. WET partially accounts for band-limited finite source frequency and shadow effects (including diffraction and scattering) in the data (Schuster and Quintus-Bosz, 1993). WET uses wavepaths aka Fresnel volumes, “fat rays” or physical rays (Červený and Soares, 1992).

As shown with synthetic data for known models (Sheehan et al., 2005; Rohdewald, 2009; Jansen, 2010; Kotyrba and Schmidt, 2014), refraction tomography and WET (with 1D starting model) work well in many situations where conventional layer-based refraction methods fail. Layer-based interpretation has problems with imaging faults, outcrops, pinch-outs and other velocity anomalies that violate the assumption of laterally continuous layers. Refraction tomography blurs sharp velocity contrasts and images them with gradients (Zelt et al., 2013).

Finite frequency effects and the resolution limit of one wavelength can explain WET blurring (Watanabe et al., 1999). The wavepaths act as low-pass or anti-alias filters to the spatial frequency content in the WET tomogram. This filtering is physically consistent with the source wavelet’s finite bandwidth (Schuster and Quintus-Bosz, 1993).

Multi-resolution tomography

Watanabe et al. (1999) propose a multi-resolution tomography analysis using the Fresnel Volume approach to get more focused tomograms with fewer artefacts. Accordingly, we improve the resolution of P-wave velocity tomograms by iteratively decreasing the WET wavepath width. Decreasing the width of wavepaths i.e. Fresnel Volumes corresponds to increasing the frequency in Fresnel Volume Tomography theory (Watanabe et al., 1999). The width of the Fresnel volume is inversely proportional to the square root of the frequency (Červený and Soares, 1992). We demonstrate our approach with the SAGEEP 2011 blind refraction synthetic traveltime data, for which the true model is known (Zelt, 2010; Zelt et al., 2013).

Processing and Results

Starting model and WET inversion, velocity update weighting

A 1D-gradient laterally averaged starting model (with horizontal layering, parallel to smoothed topography) is obtained automatically from the traveltimes, without having to assign first breaks to assumed refractors (Rohdewald, 2012). See Figure 1(a).

This starting model is iteratively refined with WET (Schuster and Quintus-Bosz, 1993) over multiple WET iterations. During one WET iteration, our Eikonal solver (Lecomte et al., 2000) forward models synthetic traveltimes, and the misfit between picked and modeled times is back-projected along wavepaths with an SIRT algorithm. We weight the velocity update in each wavepath with an undifferentiated Ricker wavelet (G.T. Schuster, personal communication, November 25, 2000); (Figure 1) and a Gaussian bell function (C.A. Zelt, personal communication, April 9, 2009); (Figure 2).

Velocity tomograms are smoothed over a grid area 5 grid columns wide and 3 grid rows high after every WET iteration. We limit the maximum velocity to 3,500 m/s during all WET runs, based on the true model (Zelt et al., 2013; Rohdewald, 2013).

Iterative refinement with multiple WET runs

For tomograms shown in Figure 1, we start with wavepaths that are 30% of one period at 50 Hz i.e. 6 ms wide (maximum delay from the fastest ray is 6 ms) and run one WET inversion with 100 WET iterations (Figure 1(b)) using the 1D starting model (Figure 1(a)). We weight wavepath velocity updates with a Ricker wavelet.

Now we iteratively decrease the wavepath width to 15%, 10%, 7%, 5%, 4%, 3% and 2%, taking the tomogram obtained with the previous WET run as the starting model for the next WET inversion (Figure 1). We also show subsurface coverage with WET wavepaths (Figure 3). Higher coverage means a more reliable interpretation for that subsurface region in (Figure 1). See our tutorial (Rohdewald, 2013) for step-by-step instructions and more figures.

Each of above eight WET runs takes 20 minutes with 100 WET iterations per run over 10,100 traces. Our WET tomography on a 2011 MacBook Air uses four threads and four CPU cores in parallel.

In Figure 2 we show the same processing as just described for Figure 1, with the only difference that we weight the wavepath velocity updates with a Gaussian function instead of a Ricker wavelet. Also, we plot Plus-Minus refractors obtained with different parameters (Figure 4 on Figure 1, Figure 5 on Figure 2).

Plus-Minus refraction interpretation

In Figure 4 and Figure 5, we also estimate refractors with layer-based Plus-Minus refraction interpretation (Hagedoorn, 1959) of the same traveltime data. We plot these refractors on the WET tomograms (Figure 1 and Figure 2).

We map first breaks to refractors interactively and semi-automatically by specifying a 1D-layered velocity model and smoothing parameters. First breaks are sorted by Common Mid-Point (CMP) vs. source-receiver offset, to obtain a quasi-continuous traveltime field suitable for reliable mapping of traces to refractors. The apparent velocity at trace-specific source-receiver offset is matched to the 1D velocity model to determine the refractor for each trace (Figure 4 and Figure 5); (Rohdewald, 2013).

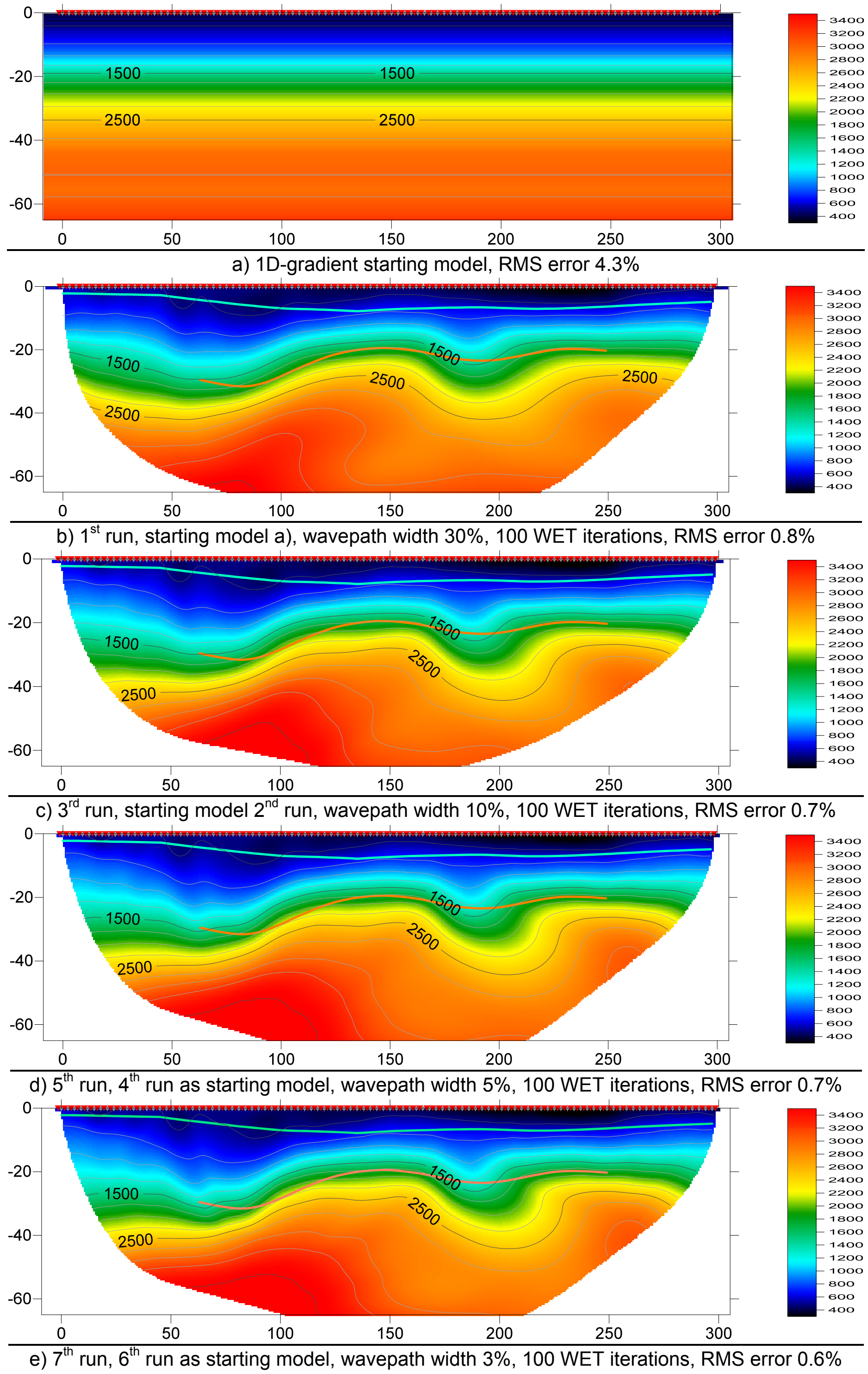

Figure 1: WET with wavepath velocity update weighted with a Ricker wavelet **(a)** 1D-gradient starting model, **(b)** velocity tomogram obtained with wavepath width 30%, **(c)** 10%, **(d)** 5%, **(e)** 3%. Color scale is velocity in m/s. Contour interval is 250 m/s. Horizontal axis is offset from first profile receiver, in m. Vertical axis is elevation in m. Overburden ***Plus-Minus refractor*** is colored turquoise, basement refractor colored orange. These two refractors are the same in (b) through (e). See Figure 4.

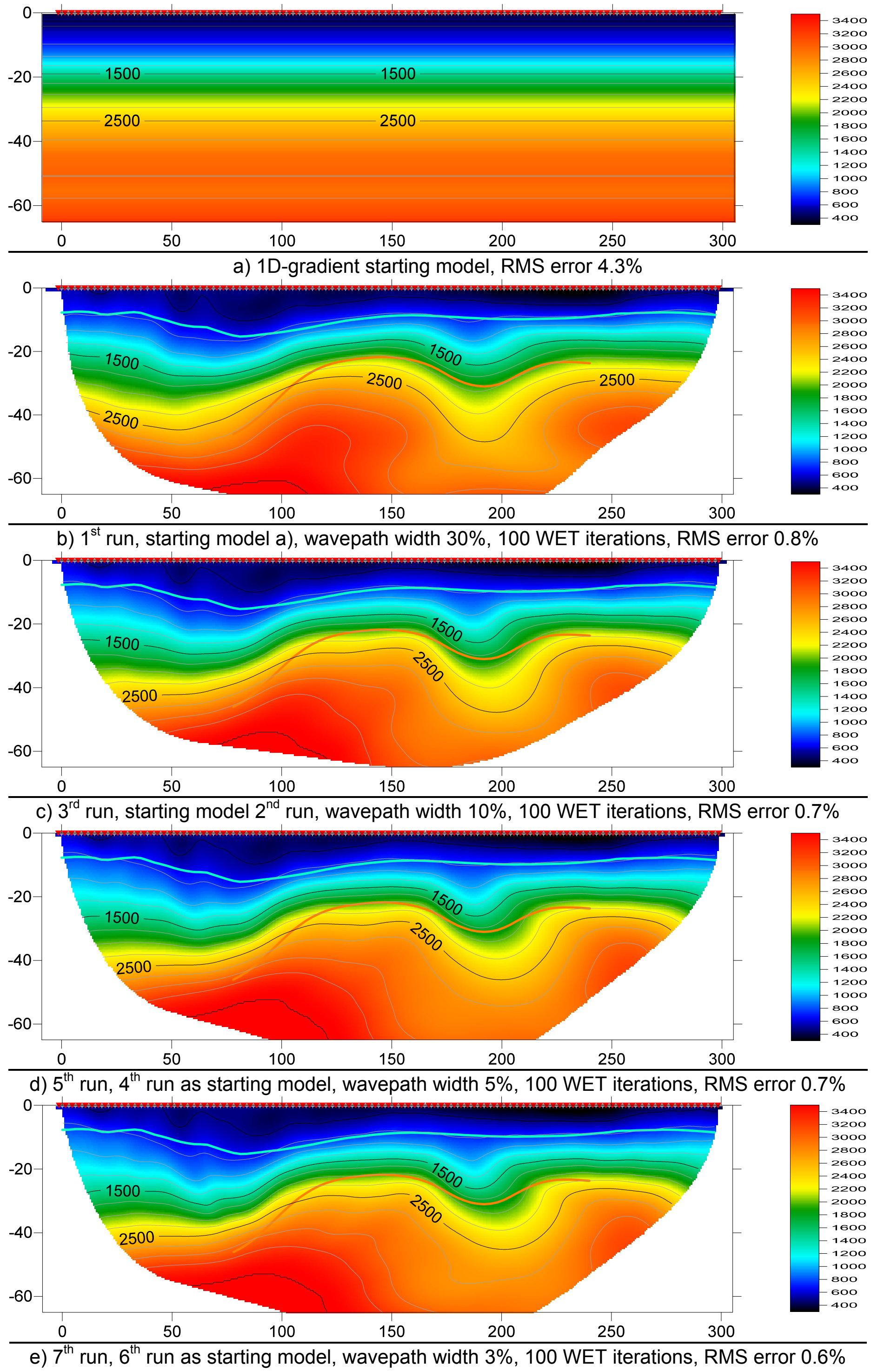

Figure 2: WET with wavepath velocity update weighted with a Gaussian function **(a)** 1D-gradient starting model, **(b)** velocity tomogram obtained with wavepath width 30%, **(c)** 10%, **(d)** 5%, **(e)** 3%. Color scale is velocity in m/s. Contour interval 250 m/s. Horizontal axis is offset in m. Vertical axis is elevation in m. Overburden ***Plus-Minus refractor*** is colored turquoise, basement refractor colored orange. These two refractors are the same in (b) through (e). See Figure 5.

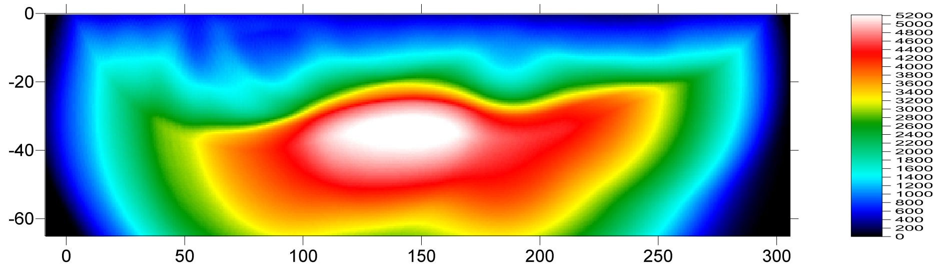

a) WET wavepath coverage for Figure 1 b), for 1st run. Wavepath width 30%.

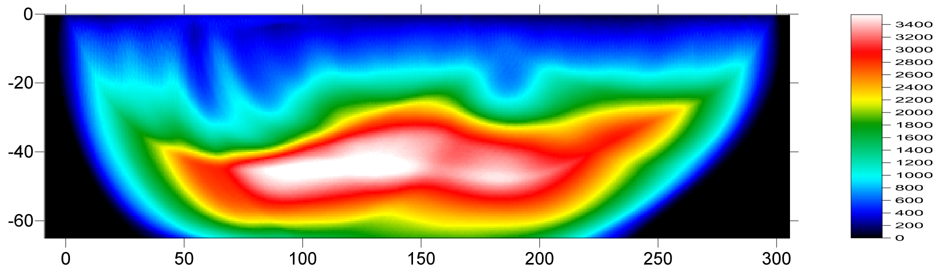

b) WET wavepath coverage for Figure 1 c), for 3rd run. Wavepath width 10%.

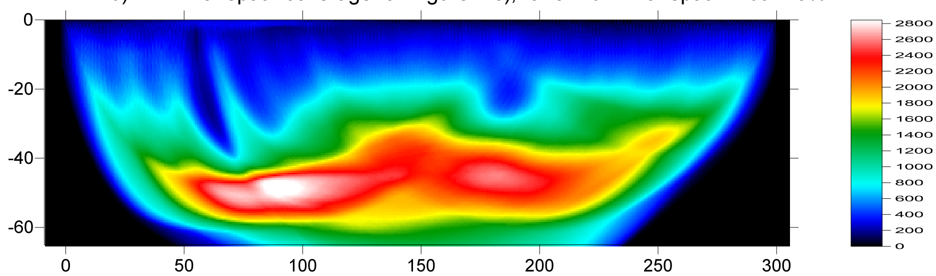

c) WET wavepath coverage for Figure 1 d), for 5th run. Wavepath width 5%.

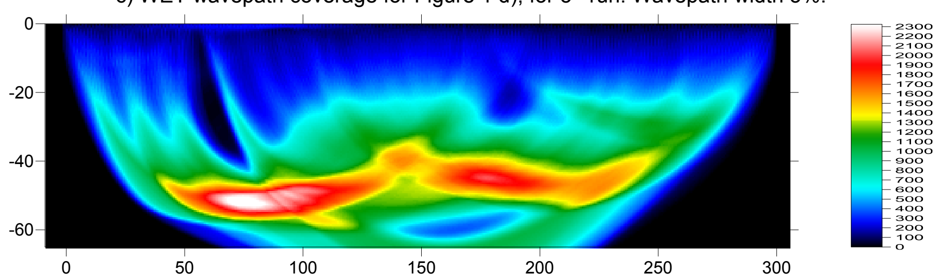

d) WET wavepath coverage for Figure 1 e), for 7th run. Wavepath width 3%.

Figure 3: WET wavepath coverage plots for steps shown in Figure 1. Color-coding is wavepaths per pixel. **(a)** WET with wavepath width 30%, **(b)** 10%, **(c)** 5%, **(d)** 3%.

In Figure 5 we increase the upper limits for layer velocity to image the refractors more deeply and better match the WET tomograms in Figure 2 than in Figure 1. We increase the CMP stack width for a laterally smoother traveltime field than in Figure 4. In addition, we increase lateral smoothing of the crossover distance in Figure 5 (Rohdewald, 2013).

Discussion

Wide wavepaths (low frequency) make WET inversion less dependent on the starting model and more robust but produce a smooth tomogram (Figure 1(b), 3(a)). Narrow wavepaths can give a sharper tomogram, but WET becomes more dependent on the starting model (previous run) and less robust.

WET images the dipping low-velocity fault zone (Zelt et al., 2013) more realistically with decreasing wavepath width (Figure 1(b) through (e), Figure 2(b) through (e)). Contours for velocity 2,500 m/s and higher velocities become more parallel to the fault zone, which dips down to the right (towards offset 250m at an elevation of -80m).

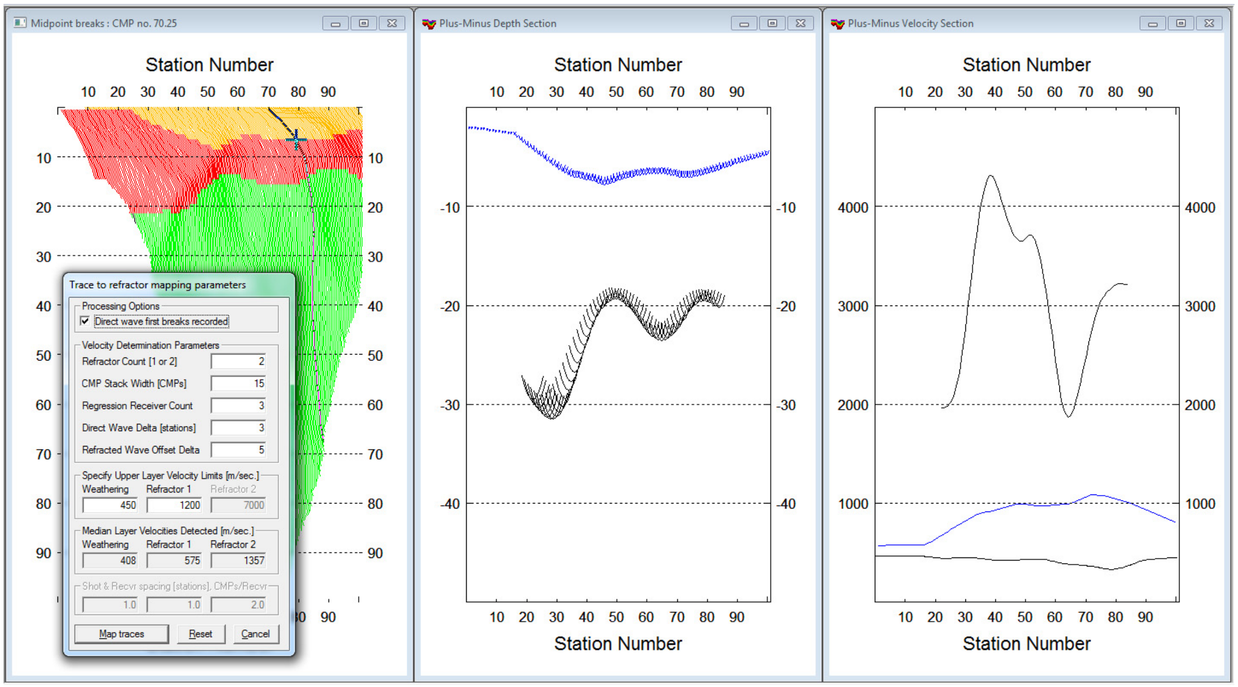

Figure 4: **(left)** Map traces to refractors in CMP-sorted first breaks display. Horizontal axis is CMP in station numbers. Vertical axis is absolute source-receiver offset in station numbers. **(center)** run time-to-depth conversion with Plus-Minus method. Horizontal axis is inline offset, in station numbers. Vertical axis is elevation in m. **(right)** display velocity section for Plus-Minus method. Horizontal axis is inline offset, in station numbers. Vertical axis is velocity in m/s.

Thin wavepaths make WET tomography more prone to generating artefacts, especially with bad or noisy first break picks and strong refractor curvature. Our velocity model (Zelt et al., 2013) causes diffraction of rays at basement corners (Figure 3(d), at offset 80m and elevation -40m).

We use the same synthetic picks for all wavepath widths (Zelt, 2010). Watanabe et al. (1999) propose to apply frequency bandpass filtering before picking first breaks, for a particular frequency and wavepath width.

For a strongly heterogeneous overburden with physical properties varying on a small scale (smaller than one wavelength, e.g. unconsolidated soil), leave wavepaths wide enough to prevent WET artefacts (stationary engraving of wavepaths in the tomogram). Consider weighting of the velocity update with a Gaussian function instead of a Ricker wavelet, in each wavepath volume (Figure 2). Gaussian weighting renders the tomogram more smoothly, which can be essential for an inhomogeneous subsurface causing strong scattering of first break energy.

At offset 150m to 250m, WET images the fault zone more clearly and deeper with Gaussian weighting in Figure 2(b), compare with Figure 1(b). At offset 80m, the vertical gradient is resolved better using Ricker wavelet weighting in Figure 1(b), with the velocity contours more closely spaced at the top of basement (elevation -40m) than in Figure 2(b). Also, the dip of the fault zone is resolved better in Figure 1(e) than in Figure 2(e).

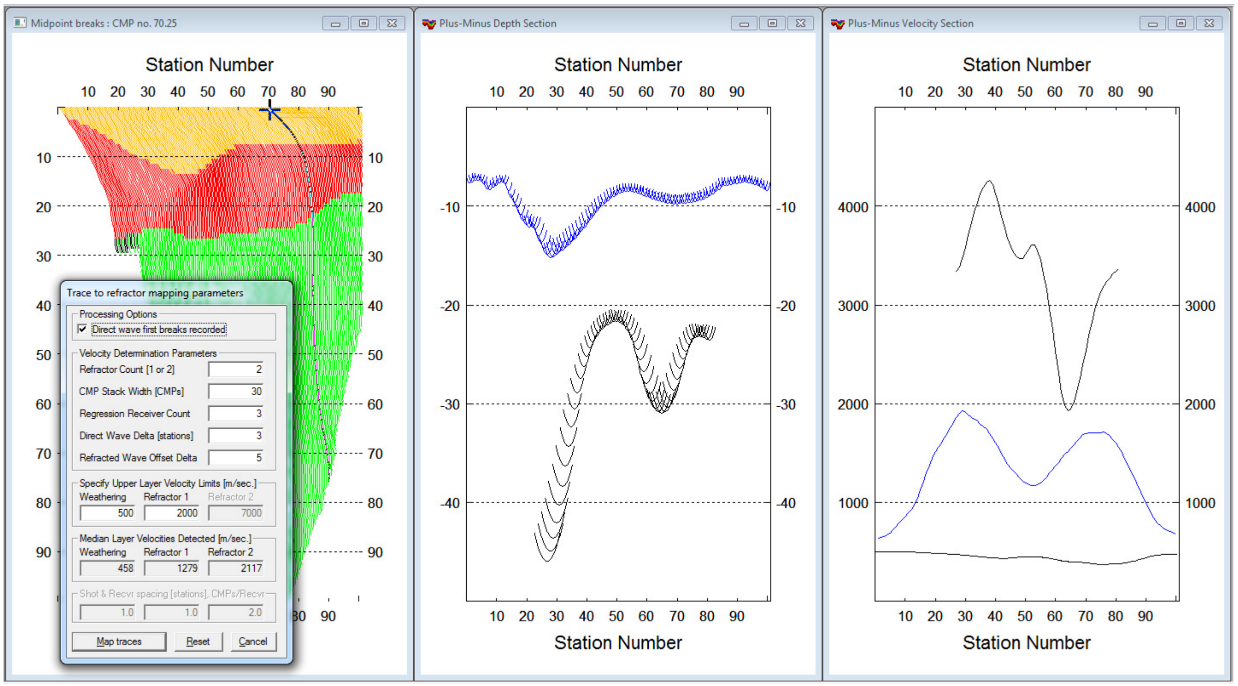

Figure 5: Same as Figure 4 but different parameters used for mapping and Plus-Minus interpretation.

As shown in Figure 4 and Figure 5, layered refraction interpretation is non-unique due to mapping traces to assumed refractors and lateral smoothing, required for refractor velocity estimation and time-to-depth conversion of refractors (Rohdewald, 2013). We match the low-velocity fault zone better in Figure 5 (station no. 65 at offset 192m), but we image the basement refractor too deeply at the basement step (station no. 30 at offset 87m).

The maximum basement velocity may not be well-constrained by the first break picks for refraction profiles, e.g. for steep synclines with the seismic line not laterally extending over the syncline's shoulders (Palmer, 2010). Limiting the basement velocity to realistic values in the starting model and during WET prevents artefacts and too deep imaging (Rohdewald, 2006; Rohdewald, 2014).

Picking at larger offsets is usually more difficult, because the signal-to-noise ratio normally decreases with increasing source-receiver offset. Resolution of refraction tomograms decreases with increasing depth below topography since rays are aligned predominantly parallel to each other at large source-receiver offsets (White, 1989). Use uphole shots to better constrain interpretation of surface-based refraction shots with improved angular coverage of rays and wavepaths (Rohdewald, 2008).

Besides showing the resolution limit of one wavelength (Watanabe et al., 1999), WET blurring also can show the uncertainty caused by bad picks, recording geometry errors, uncorrected trigger delays and out-of-plane refractions. The lower the signal-to-noise ratio, the wider the wavepaths should remain. Ray-based tomography methods tend to overfit the data and often generate artefacts (Zelt et al., 2013).

Conclusions

We have shown how to improve the resolution of P-wave velocity tomograms by iteratively decreasing the WET wavepath width. We have compared weighting the wavepath velocity update with a Ricker wavelet vs. weighting with a Gaussian function.

Plotting 1.5D Plus-Minus refractors on the WET tomogram can increase the client's confidence in the subsurface model and allows interactive adaptation of parameters, until the layered interpretation matches the 2D velocity tomogram.

Layered refraction modeling is non-unique and subjective due to mapping of traces to assumed refractors and lateral smoothing, necessary for refractor velocity estimation and time-to-depth conversion. WET interpretation depends on the maximum allowed basement velocity, which may not be well-constrained by the first break picks.

Tomograms obtained with an iterative approach of wavepath adjustment show improvement compared to the standard ray-based approach.

References

Červený, V. and Soares, J., 1992, Fresnel volume ray tracing, Geophysics, Volume 57, 902-915. http://dx.doi.org/10.1190/1.1443303 .

Hagedoorn, J.G., 1959, The Plus-Minus method of interpreting seismic refraction sections, Geophysical Prospecting, Volume 7, 158-182. http://dx.doi.org/10.1111/j.1365-2478.1959.tb01460.x .

Jansen, S., 2010, Parameter investigation for subsurface tomography with refraction seismic data, Master thesis, Niels Bohr Institute, University of Copenhagen. http://rayfract.com/papers/Thesis_Report_Stefan_Jansen_20110105.pdf .

Kotyrba, B. and Schmidt, V., 2014, Combination of seismic and resistivity tomography for the detection of abandoned mine workings in Münster/Westfalen, Germany: Improved data interpretation by cluster analysis. EAGE Near Surface Geophysics, Early Online January 2014. http://nsg.eage.org/publication/publicationdetails/?publication=72266 .

Lecomte, I.; Gjoystdal, H.; Dahle, A.; Pedersen, O.C., 2000, Improving modeling and inversion in refraction seismics with a first-order Eikonal solver, Geophysical Prospecting, Vol. 48, 437-454. http://dx.doi.org/10.1046/j.1365-2478.2000.00201.x .

Palmer, D., 2010, Non-uniqueness with refraction inversion – a syncline model study, Geophysical Prospecting, Vol. 58, 203-218. http://dx.doi.org/10.1111/j.1365-2478.2009.00818.x .

Rohdewald, S.R., 2006, Comparison of pseudo-2D DeltatV initial model with 1D-gradient initial model, for WET inversion of synthetic data set for syncline model as described by Dr. Palmer. http://rayfract.com/tutorials/palmfig3.pdf .

Rohdewald, S.R., 2008, WET inversion of refraction survey constrained by uphole shots. http://rayfract.com/tutorials/coffey04.pdf .

Rohdewald, S.R., 2009, WET inversion of synthetic data for thrust fault model. http://rayfract.com/tutorials/thrust12.pdf .

Rohdewald, S.R.; Burton, B.L.; Sheehan, J.R.; Doll, W.E., 2010, Processing of seismic refraction tomography data, SAGEEP short course notes, Keystone, Colorado, USA, April 10. http://rayfract.com/SAGEEP10.pdf .

Rohdewald, S.R., 2011, Interpretation of First−Arrival Travel Times with Wavepath Eikonal Traveltime Inversion and Wavefront Refraction Method. Proceedings of SAGEEP 2011, Charleston, South Carolina, USA, April 10 to April 14, 31-38. http://library.seg.org/doi/abs/10.4133/1.3614086 .

Rohdewald, S.R., 2012, DeltatV and XTV inversion methods, http://rayfract.com/pub/deltatv.pdf and http://rayfract.com/xtv_inversion.pdf .

Rohdewald, S.R., 2013, Tutorial showing optimized interpretation of SAGEEP 2011 blind refraction data, http://rayfract.com/tutorials/SAGEEP11_13.pdf .

Rohdewald, S.R., 2014, Model construction, WET inversion and layer-based Wavefront refraction of synthetic traveltimes for Palmer syncline model (http://rayfract.com/tutorials/palmfig9.pdf) and Mendes and Teixidó basement step model (http://rayfract.com/tutorials/step.pdf) .

Schuster, G.T. and Quintus-Bosz, A., 1993, Wavepath eikonal traveltime inversion: Theory. Geophysics, Volume 58, 1314-1323. http://dx.doi.org/10.1190/1.1443514 .

Sheehan, J.R.; Doll, W.E.; Mandell, W., 2005, An evaluation of methods and available software for seismic refraction tomography analysis, JEEG, Volume 10(1), 21-34. http://dx.doi.org/10.2113/JEEG10.1.21 .

Watanabe, T.; Matsuoka, T.; Ashida, Y., 1999, Seismic traveltime tomography using Fresnel volume approach, SEG Houston 1999, Expanded Abstracts. http://dx.doi.org/10.1190/1.1820777 .

White, D.J., 1989, Two-dimensional seismic refraction tomography, Geophysical Journal, Volume 97, 223-245. http://dx.doi.org/10.1111/j.1365-246X.1989.tb00498.x .

Zelt, C.A., 2010, SAGEEP 2011 Seismic refraction shootout: blind test of methods for obtaining velocity models from first-arrival travel times, http://terra.rice.edu/department/faculty/zelt/sageep2011 .

Zelt, C.A.; Haines, S.; Powers, M.H.; Sheehan, J.; Rohdewald, S.; Link, C.; Hayashi, K.; Zhao, D.; Zhou, H.; Burton, B.L.; Petersen, U.K.; Bonal, N.D.; Doll, W.E., 2013, Blind test of methods for obtaining 2-D near-surface seismic velocity models from first-arrival traveltimes, JEEG, Volume 18(3), 183–194. http://dx.doi.org/10.2113/JEEG18.3.183 .

Acknowledgements

We thank Colin Zelt for providing this challenging synthetic data for a complex subsurface model, and for encouraging publication of this paper. Also, we thank Curtis A. Link and Judy Paiva for their detailed reviews, edits and comments.